Reversible protein inactivation by optogenetic trapping in cells

Sangkyu Lee[1–3], Hyerim Park[2,3], Taeyoon Kyung[2], Na Yeon Kim[2], Sungsoo Kim[2], Jihoon Kim[2] & Won Do Heo[1,2]

We present a versatile platform to inactivate proteins in living cells using light, light-activated reversible inhibition by assembled trap (LARIAT), which sequesters target proteins into complexes formed by multimeric proteins and a blue light–mediated heterodimerization module. Using LARIAT, we inhibited diverse proteins that modulate cytoskeleton, lipid signaling and cell cycle with high spatiotemporal resolution. Use of single-domain antibodies extends the method to target proteins containing specific epitopes, including GFP.

The precise inhibition of target proteins can serve as an effective means to dissect complex signaling networks or to identify new therapeutic targets. Widely used genetic mutation strategies typically require a relatively long time to exhibit effects or can cause lethality early in development, which hampers studies in adult organisms[1,2]. To address these drawbacks, conditional approaches such as small molecule–based inhibition or targeted degradation have been developed to manipulate proteins after translation[3–5]. Small-molecule inhibitors work rapidly but are prone to off-target effects and offer poor reversibility and spatial resolution, especially at the subcellular level. Proteolysis-based approaches are typically irreversible and require extensive optimization of target position in the degradation machinery to accomplish effective inhibition. Optogenetic tools offer a promising opportunity for controlling signaling cascades with rapid responses, good reversibility and high spatiotemporal resolution[6–9], but most optogenetic strategies focus on protein activation.

Here we present a versatile strategy called LARIAT that inhibits protein function by reversibly sequestering targets into large, optically assembled protein architectures in living mammalian cells. LARIAT consists of two modules: a multimeric protein (MP) and a light-mediated heterodimerizer. We hypothesized that interconnections among MPs could induce the formation of higher-order protein complexes, or 'clusters'[10], that conditionally trap and thereby inactivate target proteins. Heterodimerization could be used to cluster MPs and recruit target proteins upon illumination with blue light.

The MP we chose was Ca^{2+}/calmodulin-dependent protein kinase IIα (CaMKIIα), which self-assembles into an oligomer with 12 identical subunits[11]. The C-terminal region (amino acids 315–478) is responsible for the oligomerization of CaMKIIα but lacks Ca^{2+}-responsive catalytic activity[11]. We fused CaMKIIα to CIB1 from *Arabidopsis thaliana*, which undergoes blue light–mediated interactions with cryptochrome 2 (CRY2)[8]. Upon photoexcitation, CRY2 proteins simultaneously oligomerize[9] and bind to CIB1, which form clusters by promoting interconnection among CIB1-conjugated MPs (**Fig. 1a**).

We first tested whether light-mediated CRY2-CIB1 interactions could assemble MPs into clusters. mCherry-labeled CRY2 and mCerulean-labeled CIB1-MP co-expressed in HeLa cells induced clusters (visualized as fluorescent puncta) on a timescale of seconds (the time at which a half-maximal number of clusters, ($t_{1/2}$) = 26.5 ± 2.9 s (mean ± s.d.)) upon illumination with blue light (**Fig. 1b**, **Supplementary Fig. 1** and **Supplementary Video 1**). After withdrawal of the light, the clusters disassembled within minutes (cluster decay constant τ = 5.66 ± 1.27 min (mean ± s.d.)). We could reassemble and disassemble clusters by repeated illumination (**Fig. 1b**,**c**). We observed no cluster formation in cells harboring the light-insensitive mutant CRY2(D387A)[12], and neither CRY2 nor CIB1-MP alone induced clusters (**Supplementary Fig. 2**).

Cluster formation with CRY2 alone by stimulation with light has been recently reported and used for target activation in mammalian cells[9]. In contrast, we observed negligible visible clustering in HeLa cells (0.56% of cells) when we expressed CRY2-mCherry alone under our experimental conditions (light intensities of 6.5–216.6 μW), whereas combining with CIB1-mCerulean-MPs showed remarkable clustering (95.74%) in our system (**Supplementary Fig. 3** and **Supplementary Note**). However, we do not argue against the ability of CRY2 to self-associate, as we confirmed the light-dependent and rapid homointeraction of CRY2 using the assay called emerging circle of interactive proteins at specific endosomes (ECLIPSE) (**Supplementary Fig. 4**), which visualizes specific protein interactions in endosomes[13].

Next, we examined whether clustering could be quantitatively controlled by varying light parameters. We found that total cluster area in a single cell gradually increased as the intensity or the number of pulses increased (**Fig. 1d**,**e**). In addition, pulsatile illumination repeated every 2 min could maintain the clusters (**Fig. 1f** and **Supplementary Fig. 5**). Retaining clusters

[1]Center for Cognition and Sociality, Institute for Basic Science (IBS), Daejeon, Republic of Korea. [2]Department of Biological Sciences, Korea Advanced Institute of Science and Technology (KAIST), Daejeon, Republic of Korea. [3]These authors contributed equally to this work. Correspondence should be addressed to W.D.H. (wondo@kaist.ac.kr).

RECEIVED 23 SEPTEMBER 2013; ACCEPTED 28 MARCH 2014; PUBLISHED ONLINE 4 MAY 2014; DOI:10.1038/NMETH.2940

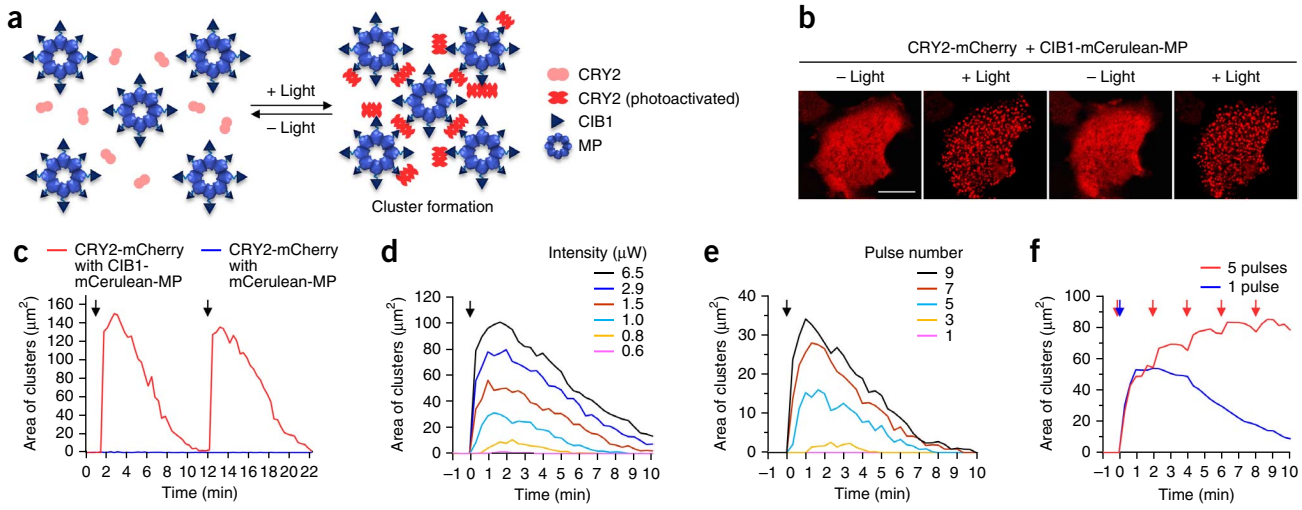

Figure 1 | Blue light–induced cluster formation. (**a**) Schematic of blue light–mediated cluster formation. (**b**) Fluorescence images of a HeLa cell coexpressing CRY2-mCherry and CIB1-mCerulean-MP illuminated with blue light twice at a 10-min interval. Scale bar, 20 μm. (**c**) Quantitative analysis of cluster formation. (**d**) Quantification of cluster formation in a single cell illuminated with light of indicated intensity. (**e**) Quantification of cluster formation at the indicated pulse number. The light intensity was fixed at 0.6 μW. (**f**) Quantitative analysis of clustering upon transient or sustained illumination with light. Arrows indicate time points of irradiation. Data are representative of two trials for each condition.

for long time periods (24 h) did not adversely affect cell viability (**Supplementary Fig. 6**).

Light can provide high spatial resolution for cluster formation. Sequential illumination showed that cluster formation is specific to the illuminated cell (**Supplementary Fig. 7a** and **Supplementary Video 2**). In addition, irradiating small subcellular regions formed clusters in highly restricted areas (**Supplementary Fig. 7b** and **Supplementary Video 3**), which could be maintained by pulsatile illumination (**Supplementary Fig. 8**). Facile spatial control could also be accomplished in specified cellular structures, such as the dendrites of hippocampal neurons (**Supplementary Fig. 9**).

We next investigated whether clusters could be used to inactivate signaling proteins. Vav2, a guanine nucleotide exchange factor that activates Rho small GTPases, induces membrane protrusion by translocating to the plasma membrane (PM)[14]. We speculated that light-induced cluster formation would functionally inactivate CRY2-conjugated Vav2 proteins by trapping them in cytosolic clusters (**Fig. 2a**). To test whether membrane-bound CRY2 could be trapped, we illuminated NIH3T3 cells coexpressing PM marker $dTomato_{PM}$, PM-targeted mCitrine-CRY2 ($mCitrine\text{-}CRY2_{PM}$) and CIB1-mCerulean-MP, and observed significant displacement of $mCitrine\text{-}CRY2_{PM}$ from the PM into clusters (**Fig. 2b** and **Supplementary Fig. 10**). Using this strategy to inactivate Vav2, we coexpressed mCitrine-CRY2-Vav2, CIB1-mCerulean-MP and mCherry-Lifeact (F-actin probe)[15] in NIH3T3 cells. Before irradiation, we observed global lamellipodia formation, whereas irradiation triggered trapping of CRY2-Vav2 in clusters followed by rapid retraction of lamellipodia, in which the activity of Rac1 small GTPase, a downstream target of Vav2, was partially attenuated (**Fig. 2c**, **Supplementary Figs. 11** and **12** and **Supplementary Videos 4** and **5**). Withdrawal of the light reversed this morphological effect and subsequent illumination induced repeated membrane retractions (**Fig. 2c**). Neither CRY2(D387A)-Vav2 nor Vav2 without CRY2 induced retraction, regardless of illumination. In addition, the presence of clusters without Vav2 also had no effect. Cells solely expressing CRY2-Vav2 did not undergo any morphological change upon irradiation, which reflects that homo-oligomerization of CRY2 is not sufficient to inhibit target Vav2 (**Supplementary Fig. 13**).

To test whether we could exert spatial control over Vav2 function, we transiently illuminated a small region of a lamellipodium, which caused it to retract and then reprotrude. In contrast, a nonilluminated region did not show any change during this period (**Supplementary Fig. 14** and **Supplementary Video 6**). In directional cell migration, the mechanism underlying communication between the front (protrusive region) and back (retracted region) of the cell is largely unknown. We therefore asked whether persistent and local inhibition of Vav2 could affect whole-cell polarity. Repeated illumination of a small region not only induced continuous membrane retraction at the treatment site; it also generated membrane protrusions on the nonilluminated opposite side of the cell (**Fig. 2d** and **Supplementary Video 7**). Kinetic analysis indicated that there was an ~3-min delay between the retraction and subsequent protrusion on the opposite side (**Fig. 2e** and **Supplementary Fig. 15a**), which implied that there might be a redirecting process during this delay. The new protrusion could be inhibited by illuminating it directly (**Supplementary Fig. 15b**), which indicated that the protrusion was Vav2-dependent. This suggests that Vav2-mediated morphological changes are involved in cross-cell coordination and that local inhibition of Vav2 is sufficient for changing cell polarity in our system.

Inactivation in our system requires CRY2 fusion to each target protein of interest. We reasoned that the versatility of LARIAT would be greatly expanded if we could take advantage of existing fusion protein collections, such as fluorescent protein (FP)-tagged cDNA libraries, and expressing strains that exist for many organisms[16–18]. To this end, we fused a GFP-binding single-domain antibody ($V_HH(GFP)$)[19] to CRY2 in order to recruit GFP-labeled proteins to CIB1-MP clusters (**Fig. 3a**). Illumination of HeLa cells coexpressing GFP, $CRY2\text{-}V_HH(GFP)$ and CIB1-MP resulted in efficient trapping of GFP in clusters,

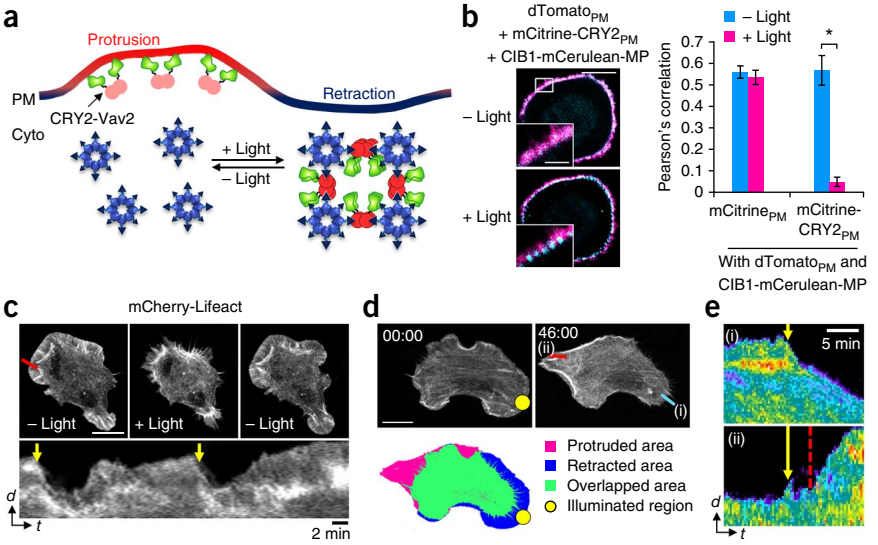

Figure 2 | Inhibition of CRY2-conjugated proteins by light-inducible trapping in clusters. (**a**) Schematic of inactivating CRY2-conjugated target proteins by light-inducible trapping in clusters. (**b**) Fluorescence images of a NIH3T3 cell showing mCitrine-CRY2$_{PM}$ redistribution from the plasma membrane into clusters upon irradiation (magenta, dTomato$_{PM}$; turquoise, mCitrine-CRY2$_{PM}$). Colocalization analysis between dTomato$_{PM}$ and mCitrine-CRY2$_{PM}$ (n = 6 cells for mCitrine$_{PM}$, 5 cells for mCitrine-CRY2$_{PM}$; *$P = 1.13 \times 10^{-6}$ by Student's two-tailed t-test; error bars, s.e.m.). Experiments were repeated twice for each set. (**c**) Fluorescence images of a shrinking of NIH3T3 cell coexpressing mCherry-Lifeact, mCitrine-CRY2-Vav2 and CIB1-mCerulean-MP upon stimulation with blue light twice at a 20-min interval. Bottom, kymograph of Lifeact corresponding to the red line in top left image. Yellow arrows indicate time points of irradiation. Images are representative of 10 trials. (**d**) Fluorescence images of a NIH3T3 cell repeatedly illuminated by blue light at 4-min intervals. The protrusion-retraction map indicates morphological changes before and after light stimulation. Time is indicated as min:s. Images are representative of 3 trials. (**e**) Kymograph of Lifeact corresponding to a blue (i) or red (ii) line in **d**. Yellow arrows and red dashed line indicate time points for irradiation and initiation of protrusion, respectively. Images in **e** are representative images from the experiment shown in **d**. Scale bars, 10 μm (2 μm in insets, **b**) and 20 μm (**c**,**d**). d, distance; t, time.

supporting our strategy. In contrast, mCherry proteins did not show any change in localization (**Fig. 3b** and **Supplementary Figs. 16** and **17**).

To examine the capability of our platform to control the activity of diverse GFP-labeled proteins, we prepared GFP-labeled Vav2, Tiam1, Rac1, Cdc42 and RhoG proteins. In all cases, we inactivated GFP-labeled target proteins in a light-dependent manner (**Fig. 3c**, **Supplementary Figs. 18** and **19**, and **Supplementary Videos 8–12**). Trapping GFP-Vav2 with an anti-GFP nanobody showed a more potent effect on membrane retraction than trapping CRY2-Vav2 (**Supplementary Fig. 20**, compare to **Fig. 2**). Next, we attempted to control activity of PI3 kinase (PI3K), which is responsible for regulating phosphatidylinositol (3,4,5)-triphosphate (PIP3) amounts at the plasma membrane. Upon illuminating cells coexpressing CFP-p110$_{CAAX}$ (PM-targeted p110) with components of LARIAT, we observed a significant ($P = 6.56 \times 10^{-7}$, 2.6×10^{-6} by Student's two-tailed t-test) reduction of PIP3 at the plasma membrane and membrane retraction (**Supplementary Fig. 21** and **Supplementary Videos 13** and **14**).

Microtubule dynamics must be tightly regulated to achieve diverse cellular functions reliably[20]. We examined whether LARIAT could inhibit microtubule function during mitosis, which typically leads to mitotic arrest or abnormal cell division. Upon illuminating HeLa cells coexpressing GFP-tubulin, CRY2-V$_H$H(GFP) and CIB1-MP for a long period of time (24 h), ~70% of cells failed to divide, whereas fewer than 10% of cells

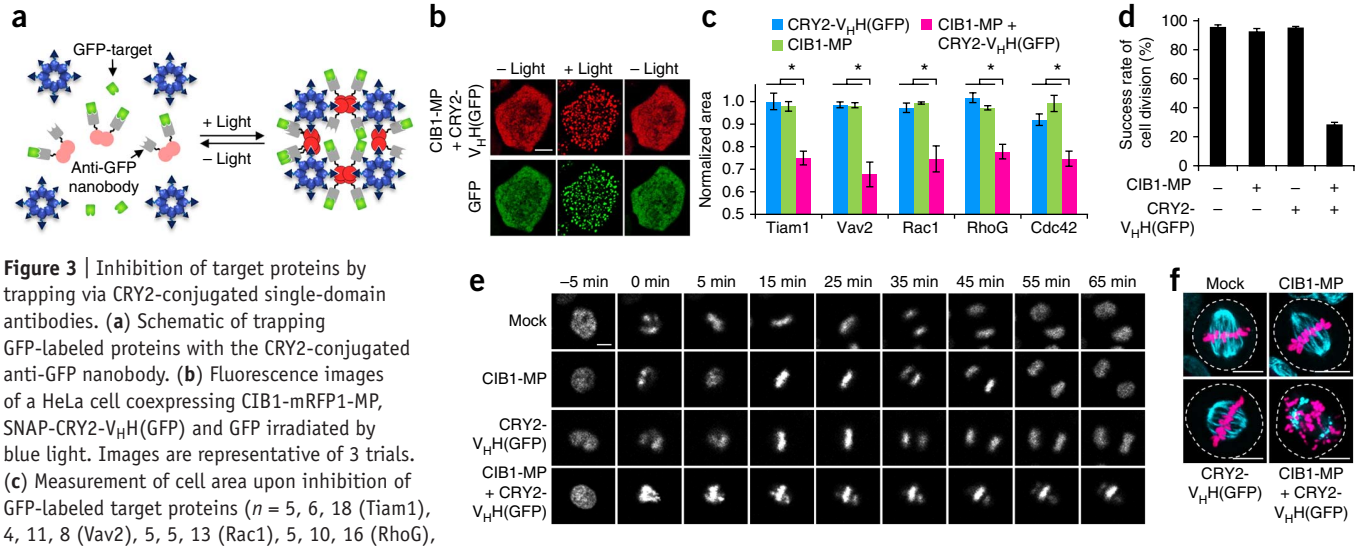

Figure 3 | Inhibition of target proteins by trapping via CRY2-conjugated single-domain antibodies. (**a**) Schematic of trapping GFP-labeled proteins with the CRY2-conjugated anti-GFP nanobody. (**b**) Fluorescence images of a HeLa cell coexpressing CIB1-mRFP1-MP, SNAP-CRY2-V$_H$H(GFP) and GFP irradiated by blue light. Images are representative of 3 trials. (**c**) Measurement of cell area upon inhibition of GFP-labeled target proteins (n = 5, 6, 18 (Tiam1), 4, 11, 8 (Vav2), 5, 5, 13 (Rac1), 5, 10, 16 (RhoG), 9, 5, 17 (Cdc42); *$P = 4.18 \times 10^{-4}$, 4.47×10^{-7} (Tiam1), 5.46×10^{-4}, 5.67×10^{-4} (Vav2), 2.13×10^{-3}, 9.99×10^{-4} (Rac1), 6.74×10^{-4}, 1.74×10^{-5} (RhoG), 8.31×10^{-5}, 4.41×10^{-3} (Cdc42) by Student's two-tailed t-test; error bars, s.e.m.). (**d**) Percentage of HeLa cells coexpressing GFP-tubulin and each indicated fusion protein that underwent cell division after illumination for 24 h (n = 6, 2, 4, 3 trials; error bars, s.e.m.). (**e**) Time-lapse imaging of mCherry-H2B for monitoring cell division. (**f**) Structure of mitotic spindles and arrangement of chromosomes on HeLa cells coexpressing GFP-tubulin, mCherry-H2B and each indicated fusion protein. Images in **e** and **f** are representative of the experiment shown in **d**. Scale bars, 20 μm (**b**) and 10 μm (**e**,**f**).

without tubulin clusters failed to divide (**Fig. 3d**, **Supplementary Fig. 22a** and **Supplementary Video 15**). Analysis of cell trajectories with mCherry-labeled histone H2B (mCherry-H2B) as a cell-cycle indicator[21] revealed that the transition from metaphase to anaphase was hampered in most cells by the tubulin trap (**Fig. 3e** and **Supplementary Fig. 22b**,**c**). The mitotic spindle structure and chromosomal arrangement were disrupted as tubulins clustered (**Fig. 3f**). Taken together, these results suggest that LARIAT can be used as a universal means to manipulate the function of GFP-tagged proteins.

We developed a versatile optogenetic method for rapidly inhibiting target proteins in a single cell on a timescale of seconds. Unlike the use of CRY2 homo-oligomerization to activate targets by increasing their local concentration[9], we demonstrated that CRY2 heterodimerization with CIB1 fused to multimeric proteins dramatically and robustly increases clustering efficiency for effective target inhibition by sequestration. Another recently reported light-inducible protein inhibition strategy in yeast cells exploits the PhyB-PIF system to sequester target proteins in organelles, away from their active sites[22]. However, sequestered proteins may still be active in organelles and lead to unintended effects. We also demonstrated that our module can efficiently inhibit diverse proteins in different cellular locations: membrane-anchored and cytosolic proteins.

The high spatiotemporal resolution and reversibility of LARIAT are valuable for investigating protein functions in the dynamic and heterogeneous intracellular environment. Tunable control of cluster formation by varying light input can be translated into quantitative perturbation of signaling networks, and the use of single-domain antibodies to target diverse endogenous proteins will expand the versatility of LARIAT[19].

METHODS

Methods and any associated references are available in the online version of the paper.

Note: Any Supplementary Information and Source Data files are available in the online version of the paper.

ACKNOWLEDGMENTS

We thank C.L. Tucker (University of Colorado) for cDNAs encoding CRY2PHR-mCherry and CIBN-pmEGFP, T. Inoue (Johns Hopkins University) for cDNA encoding YFP-PH_{Btk} and M. Matsuda (Kyoto University) for cDNA encoding Raichu-Rac1. This work was supported by the National Research Foundation of Korea Stem Cell Program (no. 2011-0019509), the Intelligent Synthetic Biology Center of Global Frontier Project (no. 2011-0031955) and the Korea Advanced Institute of Science and Technology Future Systems Healthcare Project funded by the Ministry of Science, Information and Communication Technology & Future Planning in Korea.

AUTHOR CONTRIBUTIONS

W.D.H. and S.L. conceived the idea and directed the work. S.L., H.P., T.K., N.Y.K., S.K. and J.K. performed experiments. W.D.H., S.L., H.P. and T.K. wrote the manuscript.

COMPETING FINANCIAL INTERESTS

The authors declare no competing financial interests.

1. Doupé, D.P. & Perrimon, N. *Sci. Signal.* **7**, re1 (2014).
2. Turgeon, B. & Meloche, S. *Physiol. Rev.* **89**, 1–26 (2009).
3. Stockwell, B.R. *Nature* **432**, 846–854 (2004).
4. Zhou, P. *Curr. Opin. Chem. Biol.* **9**, 51–55 (2005).
5. Banaszynski, L.A., Maynard-Smith, L., Chen, L.C. & Wandless, T.J. *Chem. Biol.* **13**, 11–21 (2006).
6. Wu, Y.I. *et al. Nature* **461**, 104–108 (2009).
7. Levskaya, A., Weiner, O.D., Lim, W.A. & Voigt, C.A. *Nature* **461**, 997–1001 (2009).
8. Kennedy, M.J. *et al. Nat. Methods* **7**, 973–975 (2010).
9. Bugaj, L.J., Choksi, A.T., Mesuda, C.K., Kane, R.S. & Schaffer, D.V. *Nat. Methods* **10**, 249–252 (2013).
10. Lee, S., Lee, K.H., Ha, J.S., Lee, S.G. & Kim, T.K. *Angew. Chem. Int. Edn.* **50**, 8709–8713 (2011).
11. Rosenberg, O.S., Deindl, S., Sung, R.J., Nairn, A.C. & Kuriyan, J. *Cell* **123**, 849–860 (2005).
12. Liu, H.T. *et al. Science* **322**, 1535–1539 (2008).
13. Lee, K.H., Lee, S., Lee, W.Y., Yang, H.W. & Heo, W.D. *Proc. Natl. Acad. Sci. USA* **107**, 3412–3417 (2010).
14. Aoki, K., Nakamura, T., Fujikawa, K. & Matsuda, M. *Mol. Biol. Cell* **16**, 2207–2217 (2005).
15. Riedl, J. *et al. Nat. Methods* **5**, 605–607 (2008).
16. Misawa, K. *et al. Proc. Natl. Acad. Sci. USA* **97**, 3062–3066 (2000).
17. Matsuyama, A. *et al. Nat. Biotechnol.* **24**, 841–847 (2006).
18. Huh, W.K. *et al. Nature* **425**, 686–691 (2003).
19. Rothbauer, U. *et al. Nat. Methods* **3**, 887–889 (2006).
20. Jordan, M.A. & Wilson, L. *Nat. Rev. Cancer* **4**, 253–265 (2004).
21. Held, M. *et al. Nat. Methods* **7**, 747–754 (2010).
22. Yang, X., Jost, A.P.-T., Weiner, O.D. & Tang, C. *Mol. Biol. Cell* **24**, 2419–2430 (2013).

ONLINE METHODS

Plasmid construction. The PCR-amplified sequence encoding association domain of CaMKIIα (amino acids 315–478)[23], indicated as MP, was cloned into pmCerulean-C1 vector (Clontech) between EcoRI and BamHI, which resulted in a plasmid encoding mCerulean-MP. In order to generate a CIB1-mCerulean-MP vector, sequence encoding CIB1 (amino acids 1–147) was inserted into the mCerulean-MP plasmid between NheI and AgeI sites. To make the plasmid encoding CIB1-mRFP1-MP or CIB1-SNAP-MP, sequence encoding mCerulean digested with AgeI and BsrGI was replaced with either mRFP1 (ref. 24) or PCR-amplified SNAP sequence (New England BioLabs), respectively. For efficient mammalian expression, sequence encoding CRY2 (amino acids 1–498) was codon-optimized. Expression plasmids for CRY2-mCherry or CRY2-EGFP were generated by inserting sequence encoding CRY2 into NheI and AgeI sites of pmCherry-C1 or pEGFP-C1 (Clontech), respectively. In order to generate mCitrine, mCherry or mCerulean-tagged CRY2 constructs, PCR-amplified *mCitrine*, *mCherry* and *mCerulean* flanked by NheI and AgeI were inserted into pmCherry-C1, and original *mCherry* was replaced with PCR-amplified sequence encoding CRY2 at AgeI and BsrGI sites. cDNA sequence encoding polybasic region of Rit (amino acids 193–219) was PCR-amplified and inserted into pmCitrine-C1 or pmCitrine-CRY2 at XhoI and BamHI sites, creating the plasmids encoding mCitrine-Rit tail or mCitrine-CRY2-Rit tail, respectively. In order to generate pmCherry-Vav2, pEYFP-Vav2, pEGFP-Vav2, pmCherry-CRY2-Vav2 or pmCitrine-CRY2-Vav2, PCR-amplified sequence encoding Vav2 (amino acids 167–541) was excised by BspEI and XhoI and inserted into each pmCherry-C1, pEYFP-C1, pEGFP-C1 (Clontech), pmCherry-CRY2 or pmCitrine-CRY2, respectively. In order to generate CRY2-mCherry-Rac1 expression vector, cDNA encoding Rac1 (wild-type) was inserted into EcoRI and BamHI sites of CRY2-mCherry plasmid. Expression plasmids for EGFP-Rac1(Q61L) and EGFP-RhoG (wild-type) were generated by inserting Rac1(Q61L) and RhoG (wild-type) into EcoRI and BamHI sites of pEGFP-C1 vector, respectively. Entry clones of Tiam1, Vav2 (full length), Cdc42(Q61L), and RhoG(Q61L) were inserted into EGFP-encoding destination vector using LR Clonase (Invitrogen). In order to generate mCerulean-CRY2-Rab5B vector, pmCerulean and sequences encoding CRY2 flanked by NheI and AgeI or AgeI and BsrGI, respectively, were inserted into CFP-Rab5B plasmid obtained from a small GTPase library[25]. For generating an expression plasmid of CRY2(D387A)-mCherry, first sequences encoding CRY2 were mutagenized through PCR-driven overlap extension, by using two mutagenic oligos and two flanking primers. Resulting PCR-amplified CRY2(D387A) was cloned at the AgeI site of pmCherry-C1. To create a plasmid encoding mCitrine-CRY2(D387A)-Vav2, PCR-amplified CRY2(D387A) from CRY2(D387A)-mCherry vector was excised by AgeI and BsrGI and inserted into mCitrine-CRY2-Vav2 vector. In order to generate the dTomato-PH_{Akt} plasmid, cDNA sequence encoding dTomato from Thy1-Brainbow-1.0l (Addgene; plasmid 18725)[26] was PCR-amplified and inserted at AgeI and BsrGI sites of pmCherry-PH_{Akt} described previously[27]. Expression plasmid for mCherry-Lifeact was generated by inserting sequence encoding mCherry into pGFP-Lifeact[15] at NheI and BsrGI sites. In order to generate a plasmid encoding mCherry-PH_{Btk}, cDNA encoding Pleckstrin homology (PH) domain of Bruton's tyrosine kinase (Btk, amino acids 1-171) was cloned into BspEI site of pmCherry-C1. To make pECFP-p110, the entry clone of p110 was inserted into ECFP-encoding destination vector using LR Clonase (Invitrogen). For the generation of expression plasmids encoding ECFP-$p110_{CAAX}$ or $EGFP_{CAAX}$, cDNA sequences encoding CAAX motif from HRas or KRas were inserted into pECFP-p110 and pEGFP-C1, respectively. To generate mCherry-CRY2-V_HH(GFP) vector, sequences encoding V_HH(GFP) from pcDNA3_NSlmb-vhhGFP4 (Addgene; plasmid 35579) was PCR-amplified and cloned into pmCherry-CRY2 at XhoI and EcoRI sites. In order to create SNAP-CRY2-V_HH(GFP) and CLIP-CRY2-V_HH(GFP) expression plasmids, sequences encoding SNAP and CLIP (New England BioLabs) were PCR-amplified and inserted into pmCherry-CRY2-V_HH(GFP) at NheI and AgeI sites, replacing sequences for mCherry. The expression plasmid for EGFP-α tubulin was generated by inserting sequences encoding tubulin from pEYFP-Tub (Clontech) into pEGFP-C1 at BsrGI and BamHI sites. The expression plasmid for mCherry-H2B was generated by inserting PCR-amplified sequence encoding histone H2B into EcoRI and BamHI sites of pmCherry-C1 (Clontech). Oligonucleotides used in this research are listed in **Supplementary Table 1**.

Cell culture and transfection. HeLa, HEK293 and NIH3T3 (ATCC) cells were maintained in Dulbecco's modified Eagle's medium (DMEM, PAA Laboratories GmbH) supplemented with 10% FBS (Invitrogen) at 37 °C and 10% CO_2. We have not recently authenticated these cell lines, but we have confirmed that they are free from mycoplasma contamination (tested with e-MycoTM Mycoplasma PCR detection kit (ver. 2.0), iNtRON). Hippocampal neurons were prepared from embryonic day 17–18 rats followed by Banker neuron culture[28], and dissociated with 0.25% trypsin and 10 mg/ml DNase. In order to remove glial cells, neurons were treated with cytosine-1-b-D-arabinofuranoside (AraC, sigma). Dissociated neurons were maintained in neurobasal medium supplemented with B27 (Invitrogen) and 2% FBS (GenDEPOT) in 5% CO_2 incubator. Cells were transfected using a Microporator (Neon Transfection System, Invitrogen) or Lipofectamine LTX (Invitrogen) according to the manufacturer's instructions, except that conditions of electroporation were optimized to increase efficiency of transfection. The optimized conditions of electroporation for HeLa, HEK293 or NIH3T3 cells were two pulses of 980 V for 35 ms, two pulses of 950 V for 35 ms or three pulses of 1,450 V for 10 ms, respectively. For live-cell imaging, cells were plated in a 96-well glass bottom microplate (Matrical Bioscience). NIH3T3 cells or neurons were seeded on a 96-well glass bottom plate coated with 100 μg/ml poly(D-lysine) (Sigma), or poly(L-lysine) (Sigma) and laminin (BD science)-treated coverglass or 6-well plates, respectively.

Live-cell imaging. Live-cell imaging was performed using a Nikon A1R confocal microscopy (Nikon Instruments) mounted onto a Nikon Eclipse Ti body equipped with CFI Plan Apochromat VC objectives (60×, 1.4 numerical aperture (NA); Nikon) along with digital zooming of Nikon imaging software (NIS-elements AR 64-bit version 3.21, Laboratory Imaging). Chamlide TC system placed in a microscope stage was used to maintain environmental condition at 37 °C and 10% CO_2 (Live Cell Instrument, Inc.). Just before imaging, the medium was replaced with OPTI-MEM (Invitrogen). Photoexcitation was delivered using a photostimulation

module in Nikon imaging software (NIS-elements) that provided three loops of 0.5-s stimuli with 488-nm lasers. A laser power setting of 6.5 μW (measured with an optical power meter from ADCMT) was used for photoexcitation, unless stated otherwise. In case of the polarity experiment, photostimulation was given with 15 loops of 0.5-s stimuli, every 4 min. HeLa cells expressing SNAP and CLIP tags were incubated with SNAP-Cell Oregon Green (New England BioLabs) or CLIP-Cell TMR-Star (New England BioLabs) for 30 min in complete medium, and washed three times with complete medium.

Emerging circle of interactive proteins at specific endosomes assay. The ECLIPSE assay was performed as described previously[13]. Briefly, fluorescence images of mCherry and mCerulean in HeLa cells coexpressing mCherry-CRY2 and mCerulean-CRY2-Rab5B (wild-type) were captured every 10 s during which CRY2 proteins were photoexcited (at 457 nm). In the experiment for monitoring reversible homo-interaction of CRY2, cells were repeatedly illuminated three times at 10-min intervals. Fluorescence intensity profiles at endosomes were analyzed as described below.

Image processing and analysis. Images were analyzed with Nikon imaging software (NIS-elements AR 64-bit version 3.21, Laboratory Imaging) and MetaMorph software (version 7.8.1.0, MDS Analytical Technologies). For quantification of cluster formation, clusters were defined as discrete puncta of fluorescence with criteria of fluorescence intensity (2,500–4,095 arbitrary units), size (>0.2 μm^2) and circularity (0.5–1.0 arbitrary units). The area of clusters per cells was measured with the "Objective Count" tool in Nikon imaging software. To quantitatively analyze the changes of fluorescent intensities and patterns in the course of cluster formation, the "Intensity Surface Plot" tool and "Time Measurement" tool in Nikon imaging software was used. Colocalization between two molecules with different fluorescent colors was quantified with Pearson's correlation coefficient by using the "Co-localization" tool in Nikon imaging software. The intensity pattern on a line was measured with the "Intensity Profile" tool in Nikon imaging software. Fluorescence intensities at designated regions of interest were measured using the "Annotations and Measurements" tool in Nikon imaging software. For cell area analysis, the "Automated Measurements" tool and "ROI Statistics" tool in Nikon imaging software were used. Regarding data in **Supplementary Figure 18b**, we divided minimal area of cells during target inactivation by initial cell area before illumination to obtain '+light' value by measuring cell areas over time. After the cell morphology was sufficiently recovered upon withdrawal of light, we divided maximal area from the recovered cell by initial area to get '–light' value. A "Kymograph" tool in MetaMorph software was used to draw kymographs. For protrusion and retraction analysis, fluorescence images of mCherry-Lifeact were converted into binary images based on intensity thresholding with MetaMorph Software. Using the "Arithmetic" tool, images of retraction were obtained by subtracting the binary images of before and after light stimulation. Regions of protrusions were conversely isolated. Areas that overlapped right before stimulation were obtained by operating "Logical AND" with the two binary images. Isolated regions were combined with the "Color Combine" tool. Statistical significance was evaluated by Student's two-tailed *t*-test.

23. Shen, K. & Meyer, T. *J. Neurochem.* **70**, 96–104 (1998).
24. Campbell, R.E. *et al. Proc. Natl. Acad. Sci. USA* **99**, 7877–7882 (2002).
25. Heo, W.D. & Meyer, T. *Cell* **113**, 315–328 (2003).
26. Livet, J. *et al. Nature* **450**, 56–62 (2007).
27. Yang, H.W. *et al. Mol. Cell* **47**, 281–290 (2012).
28. Kaech, S. & Banker, G. *Nat. Protoc.* **1**, 2406–2415 (2006).

doi:10.1038/nmeth.2940